

Article

Investigations on the Influence of Annealing on Microstructure and Mechanical Properties of Electrodeposited Ni-Mo and Ni-Mo-W Alloy Coatings

Chao Zhang ^{1,*}, Wudong Si ², Yin Wang ^{3,*}, Sichao Dai ² and Da Shu ²¹ School of Materials Science and Engineering, Nanjing Institute of Technology, Nanjing 211167, China² School of Mechanical Engineering, Anhui Polytechnic University, Wuhu 241000, China; s303537841@gmail.com (W.S.); dscwudi666@163.com (S.D.); sd@ahpu.edu.cn (D.S.)³ Guizhou Communications Polytechnic, Guiyang 551403, China

* Correspondence: zhangchao@njit.edu.cn (C.Z.); wyin3350@outlook.com (Y.W.); Tel.: +86-25-86118274 (C.Z.); +86-851-88133666 (Y.W.)

Abstract: Ni-Mo and Ni-Mo-W coatings were electrodeposited on a stainless steel sheet, and then were annealed at 200, 400, and 600 °C. The effect of annealing heat treatment on the microstructure of Ni-Mo and Ni-Mo-W electrodepositions, their nano-hardness, and tribological properties were investigated. It was revealed that the average crystalline are refined and phase separation are promoted with formation of Mo-W related intermetallic precipitates at temperature exceed 400 °C on account of the co-existence of Mo-W elements within Ni-Mo-W coatings. Annealing heat treatment leads to hardening, and the hardness and elastic module increase significantly. The grain boundary (GB) relaxation and hard precipitated intermetallic particles are responsible for the annealing-induced hardening for ≤400 °C annealed and 600 °C annealed Ni-Mo-W coatings, respectively. In addition, both adhesive wear and abrasive wear are observed for coatings, and abrasive wear becomes predominant when annealing temperature up to 600 °C. The wear resistance of coatings is improved eventually by formation of a mixture of lubricated oxides upon annealing at 600 °C and the enhancement of *H/E* ratio for ≤400 °C annealed Ni-Mo-W coatings.

Keywords: electrodeposition; Ni-Mo-W coatings; annealing; microstructure; mechanical properties

Citation: Zhang, C.; Si, W.; Wang, Y.; Dai, S.; Shu, D. Investigations on the Influence of Annealing on Microstructure and Mechanical Properties of Electrodeposited Ni-Mo and Ni-Mo-W Alloy Coatings. *Coatings* **2021**, *11*, 1428. <https://doi.org/10.3390/coatings11111428>

Received: 17 October 2021

Accepted: 17 November 2021

Published: 22 November 2021

Publisher's Note: MDPI stays neutral with regard to jurisdictional claims in published maps and institutional affiliations.



Copyright: © 2021 by the authors. Licensee MDPI, Basel, Switzerland. This article is an open access article distributed under the terms and conditions of the Creative Commons Attribution (CC BY) license (<https://creativecommons.org/licenses/by/4.0/>).

1. Introduction

The processing of nanomaterials by electrodeposition is a conventional yet one of the most effective and low-cost bottom-up methods [1], e.g., electrodeposition of Ni-P [2,3], Ni-Fe [4,5], Ni-W [6,7] and Ni-Mo [8,9] alloy coatings and their composite coatings. Ni-based metals resulting in an alloy exhibit superior mechanical and electrochemical properties. Some other studies also showed that W additions in Ni coatings can refine the grain size of deposits, and the grain size reduces with the increment of W content, providing the improvement of the strength, thermal stability, corrosion and wear resistance with serving as several applications in the field of protective coatings and micro-electromechanical systems (MEMS) [10–15]. Mo as an alloying addition is also the suitability of Ni alloy for hard chromium replacement, due to its high thermal stability, electrical and thermal conductivity amongst refractory metals and low thermal expansion coefficient [16–18]. Nevertheless, the researchers reported that when the Mo content in the deposited Ni-Mo alloy coating exceeds 25 at.%, the coating is composed of amorphous phase and exhibits micro-cracks and pits, which reduce its mechanical properties at ambient and elevated temperature [19,20]. Thus, the content of Mo in Ni-based coating is adjusted in low level to avoid micro-cracks and pits. Furthermore, some literatures reported that the addition of hard second phase particles such as ZrO₂ [21], SiC-TiN [22], Al₂O₃ [23] and diamond [24] could improve the mechanical properties of Ni-Mo coatings. Xu et al. [22] designed and

electrodeposited SiC-TiN duplex nanoparticles reinforced Ni-Mo composite coatings and revealed that the composite coatings show superior hardness and wear resistance to Ni-Mo coatings. However, since the larger volume and more various shapes of the added particles within plating bath, it is difficult to ensure the uniform distribution of the particle phase in the coatings. In view of abovementioned shortcomings, the electroplating multicomponent elements, e.g., Mo and W alloyed Ni-based coating, are conducive to further improve the mechanical properties with uniformed microstructure.

Unlike for electrodeposited binary Ni-W and Ni-Mo alloy coatings, a limited number of reports on electrodeposited ternary Ni-Mo-W coating have been published in recent studies. The research of Ni-Mo-W coatings focuses on the hydrogen absorption catalytic effect [25]. These coatings are also used as cathode for hydrogen production using electrolysis from water [26]. Considering mechanical properties of Ni-W and Ni-Mo coating, the choice of electrodeposited Ni-Mo-W alloy coatings may impart better or equivalent mechanical performance. Moreover, heat treatment is an important and necessary technology to improve the mechanical performance of Ni-based coatings, such as Ni-Mo and Ni-W [27–32]. Recently, Liu et al. [27] studied the influences of Mo content and heat treatment on the structure and mechanical properties of Ni-Mo coating, and found that an increment in hardness was derived from the grain boundary (GB) relaxation and the segregation of Mo at GB when the annealing temperature lower than the phase transition temperature. Wang et al. [28] confirmed that nano-sized NiMo precipitates dispersed in the Ni(Mo) solution matrix were responsible for the secondary annealing-induced hardening of Ni-Mo coating while the temperature ranged from 500 to 700 °C. Considering rare references of the structure evolution and strengthening mechanism of annealed ternary Ni-Mo-W coatings prepared by electrodeposition, it is necessary to research the effect of annealing temperature on the microstructure and mechanical properties of these coatings.

In this paper, both Ni-Mo-W ternary coatings and Ni-Mo binary coatings were prepared, and then annealed at 200, 400, and 600 °C respectively. The first aim of the present study was to understand the co-existence of Mo-W and annealing temperature on microstructure evolution of coatings. Subsequently, mechanical properties of Ni-Mo-W and Ni-Mo coatings were investigated as the influence of the annealing temperature. Thus, the surface morphologies, microstructure, phase composition, hardness, elastic module and tribology performance of as-deposited and annealed Ni-Mo-W and Ni-Mo coatings were analyzed and compared, and further the corresponding strengthening mechanism and wear mechanism were revealed.

2. Materials and Methods

Ni-Mo and Ni-Mo-W coatings were electrodeposited on a stainless steel sheet ($50 \times 50 \times 1 \text{ mm}^3$) as the experimental samples and control samples, respectively. Before electrodeposition, the substrate surface was polished with successive grades of sand paper. The samples were then ultrasonically cleaned and HCl solutions activated. The plating bath were prepared using distilled water and analytical-grade chemicals including $\text{NiSO}_4 \cdot 6\text{H}_2\text{O}$ (60 g/L), $\text{Na}_2\text{MoO}_4 \cdot 2\text{H}_2\text{O}$ (5 g/L), and $\text{Na}_2\text{WO}_4 \cdot 2\text{H}_2\text{O}$ (0 and 20 g/L) as metal sources for Ni-Mo and Ni-Mo-W coatings, respectively. $\text{Na}_3\text{C}_6\text{H}_5\text{O}_7 \cdot 2\text{H}_2\text{O}$ (50 g/L) and NH_4Cl (3 g/L) were used as complexing agent and conductive salt, respectively. Sodium dodecyl sulfate (SDS 0.1 g/L) and $\text{C}_7\text{H}_4\text{NNaO}_3\text{S} \cdot 2\text{H}_2\text{O}$ (Saccharin: 2 g/L) were also added to avoid pinhole and cracks in coatings, respectively. The graphite plate (99.9% purity) was applied as inertia anode. The electroplating process was carried out at the temperature of 25 °C, pH of 8, and current density of 2 A/dm² without agitation in all procedures. To maintain the composition homogeneity of coatings, the clean and dried of as-deposited Ni-Mo and Ni-Mo-W coating were annealed at temperatures of 200, 400, and 600 °C for 1 h in an operating chamber with a highly purified argon atmosphere, where the oxygen and moisture content did not exceed 1 ppm. The heating rate of 10 °C/min was utilized, and then the samples were cooled to room temperature in the furnace conditions.

The microstructures and chemical compositions of Ni-Mo and Ni-Mo-W alloy coatings (as-deposited and annealed) were analyzed by field emission scanning electron microscope (FESEM, Zeiss Merlin Compact, Jena, Germany) equipped with energy-dispersive spectroscopy (EDS, Oxford instruments X-Max 20, Oxford, UK). A transmission electron microscopy (TEM, Tecnai G2 Spirit TWIN, FEI Company, Hillsboro, CA, USA) was used to characterize the representative annealed coatings, which were prepared by the focused ion beam (FIB, FEI Company, Hillsboro, CA, USA) technique using an FEI QUANTA 3D Dual Beam, operating at beam currents from 20 to 0.1 nA. The phase composition and crystallite (grain) sizes of as-deposited and annealed coatings were analyzed by grazing incidence X-ray diffraction (GIXRD, Bruker D8 Advance, Bruker AXS Advanced X-ray Solutions GmbH, Karlsruhe, Germany) at 1° angle of incidence to the surface of the sample with a Cu K α radiation operated at 40 kV and 40 mA in ambient. The angle of diffraction ranges from 30° to 80° with a step size of 0.02°. The crystallite sizes d_{XRD} were estimated by using Scherrer's equation [33]:

$$d_{\text{XRD}} = K\lambda/\beta \cos \theta \quad (1)$$

where K is the Scherrer constant, usually $K = 0.9$; λ is the X-ray wavelength (1.5406 nm), β is the half peak width (FWHM), expressed in radian unit rad; θ is the Bragg diffraction angle.

The nano-hardness and elastic modulus values were estimated based on the Oliver-Pharr method [34] using a Berkovich indenter (Agilent Technologies, Santa Clara, CA, USA) on an Agilent G200 nanoindentation tester (Agilent Technologies, Santa Clara, CA, USA) at the maximum force 200 mN and loading and unloading rate: 50 mN/s, respectively. At least 10 independent measurements were performed on each sample in different areas of the coating surface. The tribological properties in a rotary ball-on-disk configuration was evaluated by the friction and wear tester (RTEC MFT3000, RTEC INSTRUMENTS, San Jose, CA, USA). Reciprocating ball-on-disk tests were carried out in air to determine the friction and wear properties of as-deposited and annealed coatings under dry friction condition at room temperature. All samples slid against 52,100 ball (a diameter of 6.35 mm) at the load of 2 N and the frequency of 5 Hz. The wear rate (W_r) of the coatings was calculated using the equation of $W_r = W_v/(F_n \times L)$, where W_v is the worn volume in mm³, F_n is the normal force applied, and L is the sliding distance [35]. The volume loss was determined from the cross-sectional area, profiled by the confocal laser scanning microscope (Olympus OLS4100, Olympus, Tokyo, Japan), and the perimeter of the wear track.

3. Results and Discussion

3.1. The Microstructure

The EDS analysis results of as-deposited Ni-Mo and Mo-Mo-W coatings are listed in Table 1, the impacts of Na₂WO₄·2H₂O addition on Mo and W contents are observed in Ni-Mo-W coating. With the occurrence of Na₂WO₄·2H₂O in plating bath, the Ni content drops, while Mo content changes mildly in the being formed Ni-Mo-W coating. As reported of induced co-deposition principle of Ni-Mo-W coating [36], the electrodeposition process would be promoted with the increase of the concentration of Na₂WO₄·2H₂O as the competition relation in the deposition process of Mo and W. Moreover, the graphite anode rather than nickel anode is employed in this experiment, the concentration of nickel ion in electroplating bath is constant. The nickel (II) ions are insufficient to satisfy the requirement for induced co-deposition as the reduction of tungstate radical ions in the bath with the increasing of W content, leading to the decline of Ni content in the coating.

Table 1. The concentration of Na₂WO₄·2H₂O in plating bath and EDS analysis results of as-deposition coatings.

Coatings	Na ₂ WO ₄ ·2H ₂ O Concentration	Ni (at.%)	Mo (at.%)	W (at.%)
Ni-Mo	0 g/L	81.9	18.1	0
Ni-Mo-W	20 g/L	75.4	16.9	7.7

A series of XRD patterns for as-deposited and different temperatures (from 200 to 600 °C) annealed Ni-Mo coatings and Ni-Mo-W coatings are presented in Figure 1a,b, respectively. It can be seen the absence of Mo peaks or Mo-W peaks on the XRD spectra of as-deposited Ni-Mo and Ni-Mo-W coatings. Mo atoms or Mo-W atoms with larger radius are dissolved in the lattice of Ni, showing face-centered cubic (supersaturated) solid solution in as-deposited coatings. In comparison of Ni-Mo coating, the peaks of Ni(Mo,W) solid solution shift to smaller 2θ values due to a larger expanding of the lattice constant in Ni crystal with co-existence of both W and Mo atoms for ternary Ni-Mo-W coating. Ni-Mo-W coating in as-deposited state exhibits the broadening peaks of Ni(Mo,W) solid solution as reflected reduction of average crystallite size estimated from XRD results. This reveals that the crystalline can be refined with incorporation of W element for Ni-Mo coating. After annealing, the average crystallite sizes of all the coatings increase slightly up to 400 °C as shown in Figure 1c, which is deduced to initial annihilation of dislocations and subsequent grain boundary relaxation. When the temperature is lower than 400 °C, the (111) orientations of Ni(Mo) or Ni(Mo,W) solutions are dominated, and the sharpening of higher-order Ni peaks corresponding to (200), (311) and (222) planes exhibit more obvious with the increase of annealing temperature. A further grain boundary relaxation is considered as a reason of these effects correlated with the grain growth and grain boundary segregation of Ni-based coating reported in ref. [37]. No other peaks are found for Ni-Mo coating annealing at no more than 400 °C without phase separation occurred. It is worthy to note that the peak ascribed to the Ni₄W intermetallic phase is presented on the diffraction pattern of 400 °C annealed Ni-Mo-W coating. This is inconsistent with Ni-W binary phase diagram for presence of Ni₄W intermetallic phase when W content less than 12 at.%, indicating that the Mo-W co-added in Ni-based solid solution promotes the precipitation of W-related intermetallic compounds at lower temperature. Upon post-annealing at 600 °C, the appearance of new peak corresponding to Ni₃Mo intermetallic phase is observed with the narrow and sharpen peaks for Ni-Mo coating. Meanwhile, XRD results reveal that 600 °C annealed Ni-Mo-W coating shows phase separation obviously with precipitating both Ni₃Mo and Ni₄W intermetallic phases, and grain coarsening with size of 37 nm, which is inferior to that of corresponding Ni-Mo coating. This suggests that Mo-W co-existing facilitates in grain refinement of Ni-based coatings due to grain boundaries segregations of refractory atoms [38] and intermetallic precipitations playing as the grain growth inhibitor within Ni-Mo-W alloys.

As shown in Figure 2a, the cross-sections SEM observations of the representative 600 °C annealed Ni-Mo-W coating confirm that the coating with layer thickness about 15 µm is crack-free and adhered well to the stainless steel substrate. In general, qualitative analysis of the chemical composition along the scan line (parallel to the direction of the coating growth) is demonstrated in Figure 2b, proving the composition homogeneity for coatings annealed at 600 °C. The tiny gradual fluctuations of relative proportion among Ni, Mo, and W in the coatings, and the slight diffusion of Fe from the substrate into the layer and Ni in the opposite direction, are observed.

The SEM micrographs illustrating surface morphologies of as-deposited and annealed Ni-Mo alloy coatings are presented in Figure 3. From the SEM images it can be observed that as-deposited Ni-Mo coatings exhibit dense and nodular surface morphology. For annealed Ni-Mo coatings, the changing from fine nodular to coarse granular surface morphology with increasing annealing temperature in Ni-Mo coatings can be attributed to crystalline growth, which is confirmed by XRD results. Note that the significant increment of the sizes is observed for the larger granular structures in surface morphology as shown in Figure 3c,d, indicating that abnormal grain growth happens at both 400 and 600 °C annealed Ni-Mo coatings. This can be deduced that the granular structures grow continually and the sizes of granular structures are large enough to contact and then aggregate each other with forming the inhomogeneous bigger granular structures when annealing exceed 400 °C. In additions, the scattered tiny white particles can be observed in Figure 3d.

Combined with the XRD analysis results, it can be inferred that the white particles reside as the precipitation of Ni_3Mo intermetallic compound phases.

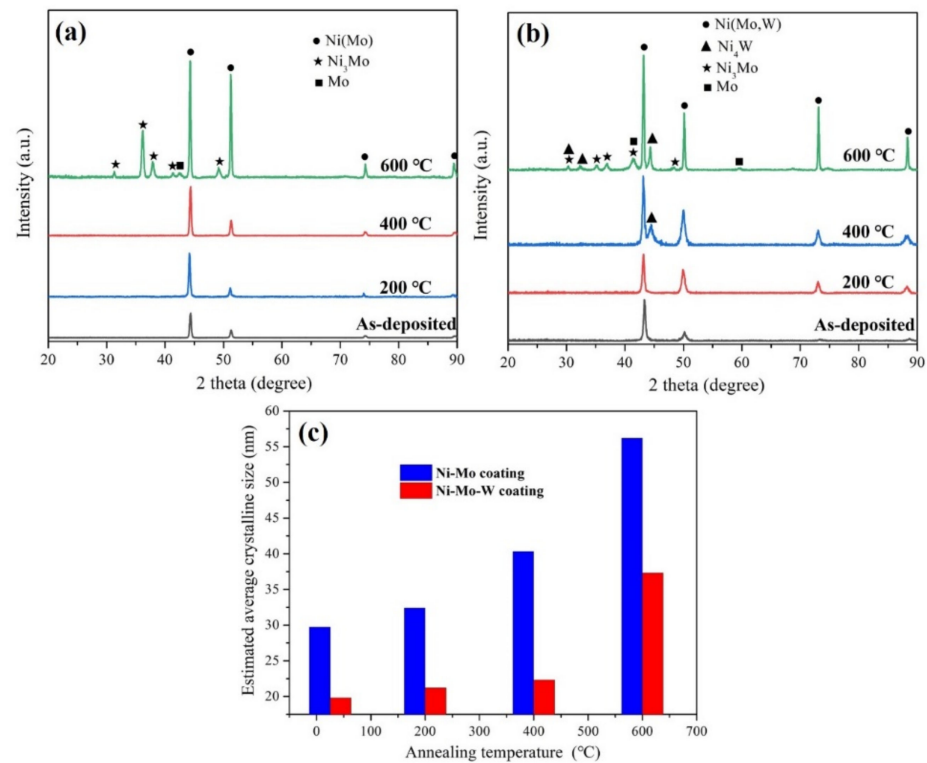


Figure 1. X-ray diffraction patterns of as-deposited and annealed coatings in the temperature range from 200 to 600 °C: (a) Ni-Mo coatings; (b) Ni-Mo-W coatings, and (c) Estimated average crystalline size using Scherrer equation from XRD results.

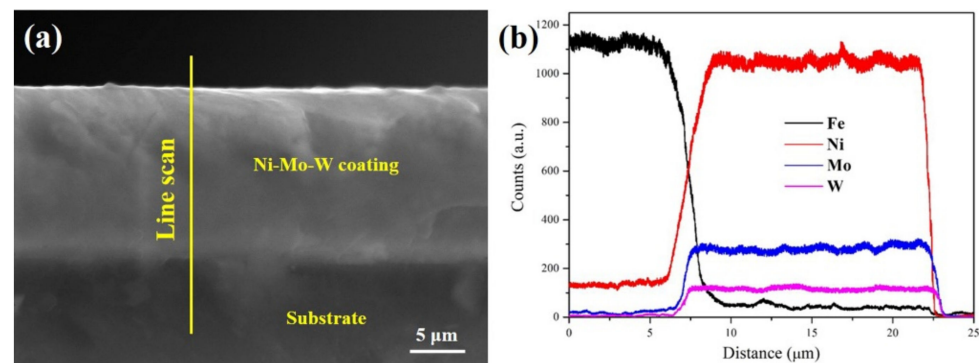


Figure 2. (a) The cross-section of SEM micrographs of the representative 600 °C annealed Ni-Mo-W coating and (b) with corresponding qualitative chemical analysis (EDS) along the line of scans (profiles of Ni, Mo, W and Fe counts).

The SEM surface morphologies of Ni-Mo-W coatings as-deposited and annealed ranging from 200 to 600 °C are shown in Figure 4. The coexistence of W-Mo element has an obvious influence on the surface morphologies of the as-deposited and annealed coatings. As shown in Figure 4, the morphology of both as-deposited and annealed Ni-Mo-W coatings displays smoother surfaces with the growth of smaller crystals, and there seems that a denser structure is provided in comparison with the morphologies of Ni-Mo coatings in the same annealing states. This case can be account for more nucleation sites on the Ni-based coatings with incorporation of more Mo and W contents, and thus Ni-Mo-W

coatings show inferior roughness and grains size. It can be also observed that Ni-Mo-W coatings after annealing lower than 400 °C perform nodules-type morphology as the presence of nanocrystalline phase. This nodules-type structure transforms into cauliflower-type morphology with the temperature increasing to 600 °C. This can be attributed to the more columnar crystals growth of Ni-based solid solutions [27]. Similar to 600 °C annealed Ni-Mo coating, it is obvious that fine and dispersed white particles appear on the surface morphology of both 400 and 600 °C annealed Ni-Mo-W coatings. Those white particles may be involved to phase separation to obtain sophisticated relevant intermetallic compounds phases for 400 and 600 °C annealed Ni-Mo-W coatings, and hence it is essential to further investigate by TEM characterization and analysis.

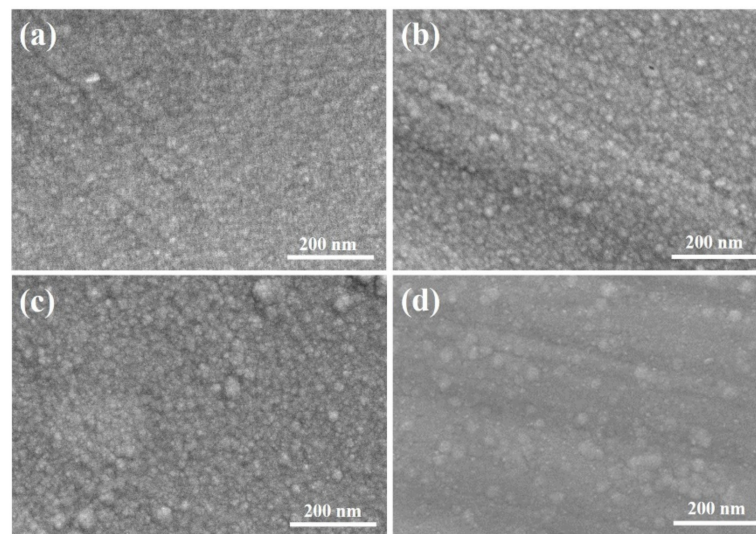


Figure 3. SEM surface micrographs of Ni-Mo coatings: (a) as-deposited and annealed at (b) 200 °C, (c) 400 °C and (d) 600 °C.

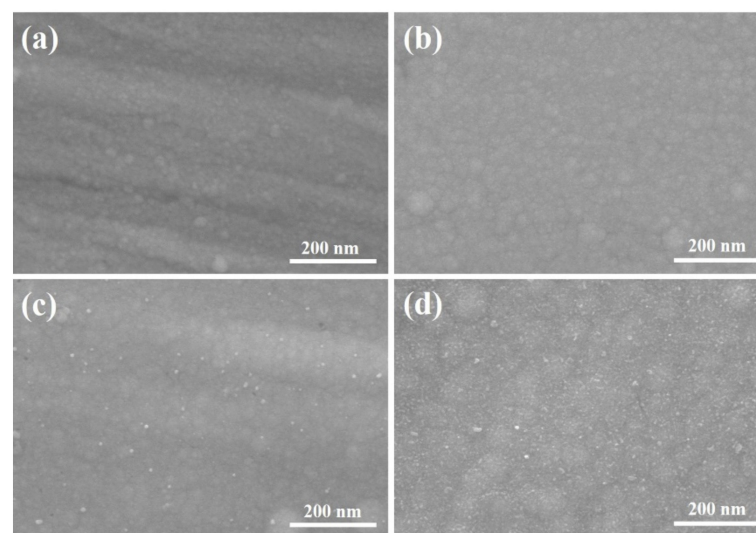


Figure 4. SEM surface micrographs of Ni-Mo-W coatings: (a) as-deposited and annealed at (b) 200 °C, (c) 400 °C and (d) 600 °C.

The TEM images and grain size distribution of Ni-Mo-W coating after annealing at 400 °C is illustrated in Figure 5. It can be seen from the bright field images (Figure 5a) that the coating consists of nanocrystalline. The corresponding electron-diffraction pattern of coating in Figure 5b shows that the existence of Ni(Mo,W) solution in major, which is consistent with the results of XRD as demonstrated in Figure 1b. The grain size of 400 °C

annealed Ni-Mo-W coating ranges from 0 to 90 nm as shown in Figure 5c, and the average size is about 28.2 nm which is slight higher than the calculated value by XRD in Figure 1c. This may be attributed that entire sub-grains inside the coatings with lower dimensions are hardly measured by TEM observation. The representative nano-grain as Ni(Mo,W) solution can be found in the region marked A within HRTEM image of Figure 5d, and the orientation of these grains is Ni(Mo,W) (111) plane. Moreover, the fine crystallized domain with a size of about 20 nm in length is found in the labeled B region of Figure 5d, showing a spacing of about 0.208 nm of the lattice fringes extracted from FFT and corresponding IFFT results, which is in accordance with the (211) plane of Ni₄W intermetallic phase. It is indicated that the onset temperature for phase separation of Ni(Mo,W) solution with formation of Ni₄W intermetallic precipitation is smidgen lower than 400 °C in annealed electrodeposition of Ni-Mo-W ternary coatings.

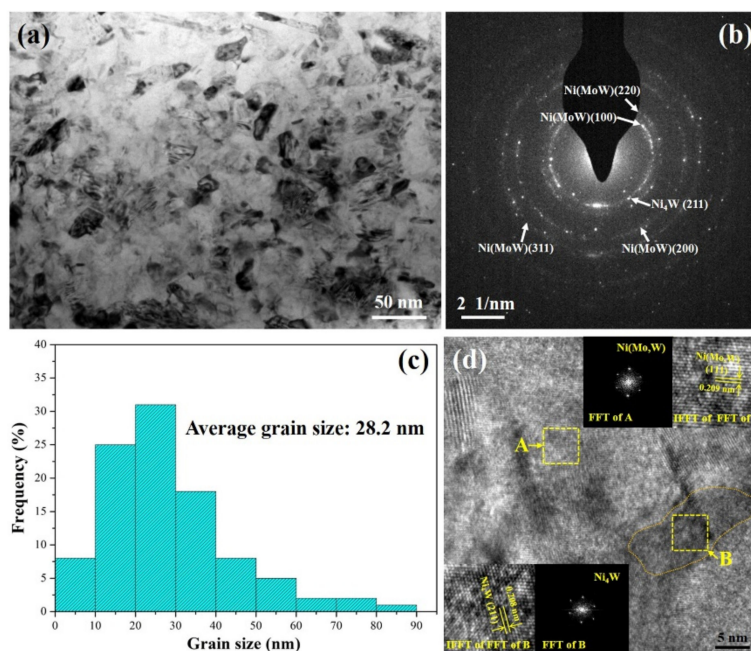


Figure 5. TEM images of the Ni-Mo-W coating annealed at 400 °C: (a) Bright-field image, and (b) corresponding selected area diffraction (SAD) is shown in inset of (a); (c) Grain size distribution represented in histogram; (d) HRTEM image, and insets of (d) are respectively the fast Fourier transformation (FFT) results and corresponding inverse fast Fourier transform (IFFT) results of the square regions marked A and B.

Figure 6 illustrates BF-TEM images and grain size distribution of Ni-Mo-W coatings after annealing at 600 °C. The grains in the bright field images (Figure 6a) exhibit crystallized and coarsened completely, and the diameter of the coating ranges from 20 to 80 nm. Both the Ni(Mo,W) solution and intermetallic compounds phases, e.g., Ni₃Mo and Ni₄W, are presented in the discrete spots in corresponding SAD patterns of Figure 6b. Figure 6c presents the grain sizes distribution of the Ni(Mo,W) matrix and precipitated phases in 600 °C annealed Ni-Mo-W coating. The size of them is in the range of 10~110 nm with the average size of about 52.5 nm, which is bigger than that in Figure 5c due to the promotion of grain growth by increasing annealing temperature. Further analysis using HRTEM allows confirmation of significant changes in precipitated phases of 600 °C annealed Ni-Mo-W coating as shown in Figure 6d. Figure 6e–g illustrates that the corresponding IFFT of FFT results of the square regions marked A, B and C in darker contrast in Figure 6d reveals Ni₃Mo intermetallic phase within marked A and B regions and Ni₄W intermetallic phase within marked C region, respectively. In addition, Ni(Mo,W) solution phase are identified for the labeled D region in brighter contrast in Figure 6d. Based on HRTEM analysis, it is deduced that Ni₃Mo and Ni₄W intermetallic phase are precipitated, and then are coarsened

to form larger and denser dispersed nano-particles involving in phase separation of 600 °C annealed Ni-Mo-W coating.

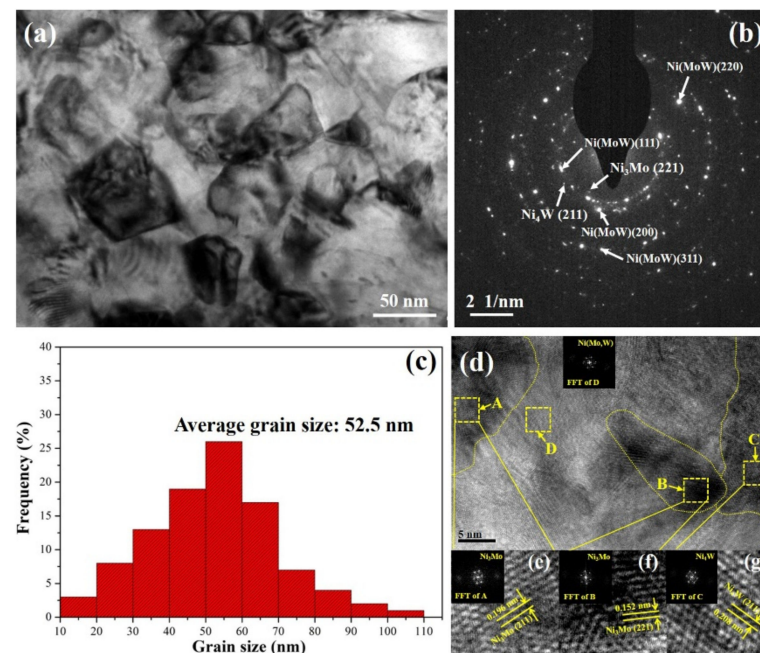


Figure 6. TEM images of the 600 °C annealed Ni-Mo-W coating: (a) Bright-field image, and (b) corresponding selected area diffraction (SAD) is displayed in inset of (a); (c) Grain size distribution represented in histogram; (d) HRTEM image, and FFT result of labeled D region is shown in inset of (d); (e), (f) and (g) are in response to IFFT of FFT results of the square regions marked A, B, and C, which are shown in inset of (e), (f) and (g), respectively.

3.2. Mechanical Properties

Figure 7 shows the hardness and elastic modulus values measured by nano-indentation of both Ni-Mo and Ni-Mo-W coatings as a function of the annealing temperature. It can be clearly observed that the increment in hardness ranging from 0.8–2.3 GPa are obtained for Ni-Mo-W coating in compared with Ni-Mo coatings at the same annealing temperature. In the case of as-deposited and annealed Ni-Mo-W coatings, three different factors may be associated with the enhancement of hardness, namely, solid solution strengthening and grain refinement, and precipitation strengthening [8,27,28,30,31]. As discussed in the relevant literatures [37,38], refractory metals such as W and Mo additions in Ni-based coatings cause little change in solid solution strengthening. The interaction between dislocations with the symmetric strain field induced by additions of substitutional elements for nanocrystalline Ni-based coatings are weak, showing small effect of solid solution strengthening [39]. Moreover, the hardness of coatings is enhanced by reduction of grain size due to a significant increase of intercrystalline volume fraction [40] according to Hall-Petch (H-P) relation, which could be attributed to the very slow diffusion of Mo and W atoms in Ni-Mo-W coatings on the basis of diffusional creep and grain boundary sliding theory [39]. After annealing exceeds 400 °C, Ni₄W and successive Ni₃Mo precipitations formed by phase separation can be regarded as the hardening phase in comparison of the Ni(Mo,W) solution phase. The Orowan mechanism can be contribute to the increase in strength by means of rendering the dislocations bypass the harder precipitates [41]. On the other hand, annealing-induced hardening of both Ni-Mo and Ni-Mo-W coatings are obtained. While the annealing temperature is lower than the onset temperature of phase separation, the remarkable increments in hardness could be ascribed to grain boundary relaxation with annihilation of excess dislocations at the grain boundary, which are transforming to a more stable configuration without obvious grain growth [27,30,37]. It is worthy to note that the

hardness of the coatings shows slight improvements with annealing temperature up to 600 °C. The fact of a lower contribution to the H-P strengthening component in coatings are substantiated due to grain coarsening on annealing [27,31], and the hardness can be compensated by the strengthening effect of the fine Ni₃Mo or Ni₃Mo-Ni₄W precipitates resulting from phase separation.

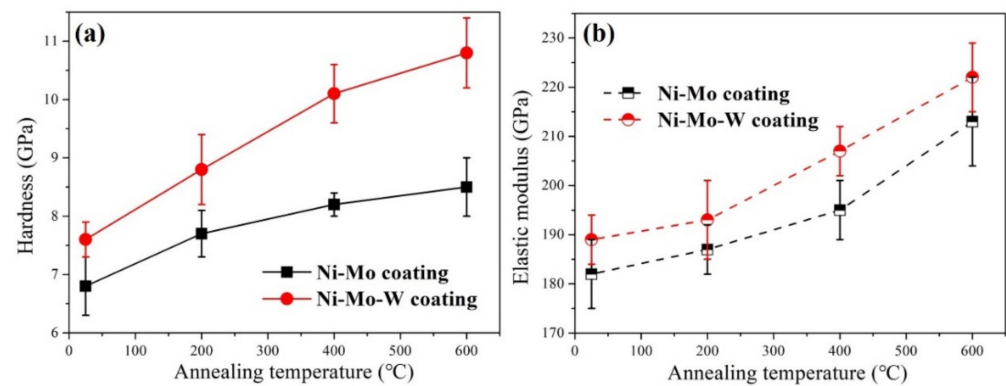


Figure 7. The nano-indentation measured mechanical properties of as-deposited and 200 to 600 °C annealed Ni-Mo and Ni-Mo-W coatings: (a) Hardness; and (b) elastic modulus.

Figure 7b shows the comparison curve of elastic modulus for Ni-Mo and Ni-Mo-W coatings with annealing temperature. Primarily, it can be observed that Ni-Mo-W coatings show higher elastic modulus compared with Ni-Mo films at the same annealing temperature due to stronger solid solution effect with W addition [8]. The elastic modulus of coatings is enhanced significantly upon annealing at 600 °C, this can be attributed to the fact that the precipitations of intermetallic phase exhibit a superior elastic modulus (Ni₄W: 234 GPa [42]; Ni₃Mo: 230 GPa [42]) compared to Ni (198 GPa [42]).

Figure 8 shows the friction coefficient curves of Ni-Mo and Ni-Mo-W coatings at different annealing temperatures sliding against 52,100 ball. The typical curves of friction coefficient are observed with obvious running-in process for as-deposited and annealed ≤ 400 °C Ni-Mo and Ni-Mo-W coatings. On the contrary, the absence of running-in stage of 600 °C annealed Ni-Mo and Ni-Mo-W coatings are presented, owing to the shorter time of compacting shallow worn tracks of harder coatings subjected to 52,100 ball. In addition, the friction coefficient of the stable-stage decreases gradually with the increase annealing temperature up to 400 °C, and then drop below 0.4 for 600 °C annealed coatings. This may be ascribed to the upgrading of hardness at elevated annealing temperature.

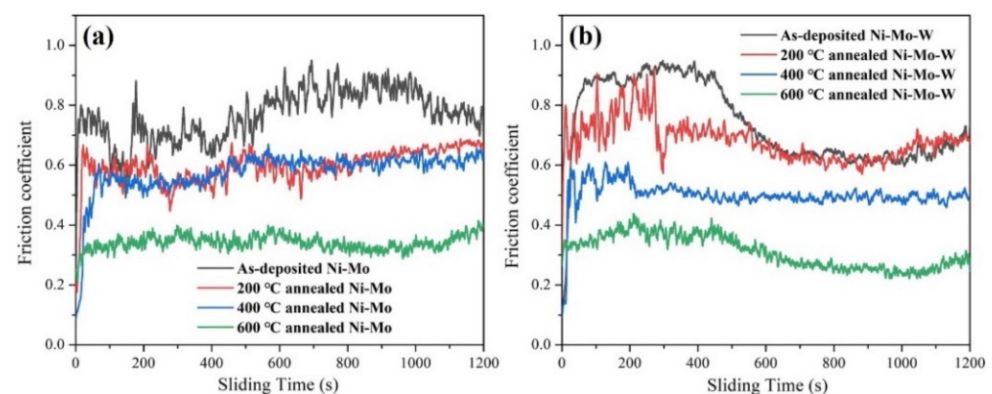


Figure 8. The curves of friction coefficient vs. sliding time for as-deposited and 200 to 600 °C annealed: (a) Ni-Mo coatings; (b) Ni-Mo-W coatings.

Figure 9 displays the influence of annealing temperature on the friction coefficient and the wear rate of Ni-Mo and Ni-Mo-W coatings. The values of friction coefficient reduce significantly with the increase of annealing temperature for both Ni-Mo and Ni-Mo-W coatings, implying the evolution of wear mechanism for annealed coatings. The wear rate is also found to be decreasing with increase in annealing temperature and the inferior values of wear rate are provided for Ni-Mo-W coatings in same annealing condition as evident in Figure 9b. As list in Table 2, for coatings annealed at ≤ 400 °C, this coincides with the results of previous reports that the wear resistance of coatings is improved with the enhancement of H/E ratio determined from the values of hardness and elastic modulus [43,44]. Meanwhile, H/E ratios are reduced for 600 °C annealed coatings, implying other reasons may affect wear resistance of these coatings.

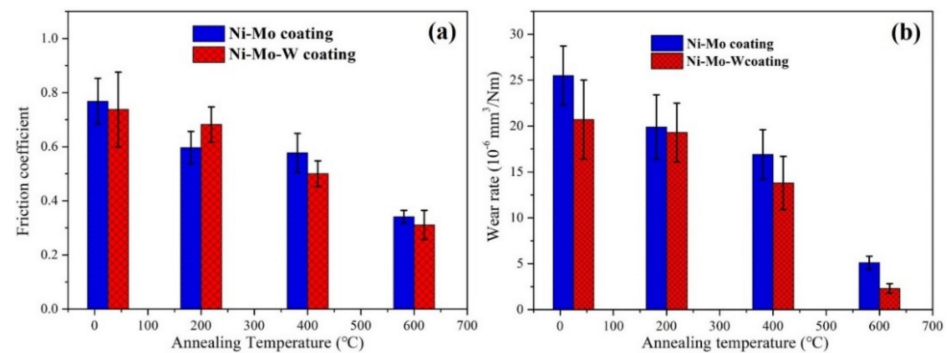


Figure 9. Friction coefficient and wear rate of Ni-Mo and Ni-Mo-W coatings with varying annealing temperatures. (a) friction coefficient; (b) wear rate.

Table 2. The H/E ratio determined from the values of hardness and elastic modulus of as-deposited and annealed Ni-Mo and Ni-Mo-W coatings in Figure 7.

Annealing Statements	Coatings	H/E
As-deposited	Ni-Mo	0.03736 ± 0.00435
	Ni-Mo-W	0.04021 ± 0.00272
200 °C annealed	Ni-Mo	0.04118 ± 0.00333
	Ni-Mo-W	0.04560 ± 0.00521
>400 °C annealed	Ni-Mo	$>0.04205 \pm 0.00239$
	Ni-Mo-W	0.04879 ± 0.00368
600 °C annealed	Ni-Mo	0.03991 ± 0.00421
	Ni-Mo-W	0.04865 ± 0.00437

The SEM worn surface morphologies of as-deposited Ni-Mo and Ni-Mo-W coatings and annealed in different temperatures are shown in Figure 10. It can be illustrated that the width of wear track becomes narrow with increasing annealing temperature particularly in 600 °C annealed Ni-Mo-W coatings, indicating that the wear resistance of coatings is improved with Mo-W co-existence and annealing heat treatment. The wear mechanism of both adhesive and abrasive in character can be deduced to the intense chipping of the superficial material of coatings [30], which is visible on the worn tracks of as-deposited coatings and annealed in temperature ≤ 400 °C. Meanwhile, fluctuations of the friction coefficient can be observed in the friction coefficient curve especially for as-deposited coatings, and thus the higher wearing losses are provided by presence of wider grooves. On contrary, for Ni-Mo and Ni-Mo-W coatings annealed at 600 °C, the wear character changes into typically abrasive, owing to occurrence of plough groove [45]. This case is consistent with the results of stable friction coefficient and lower friction coefficient for 600 °C annealed coatings as shown in Figure 9.

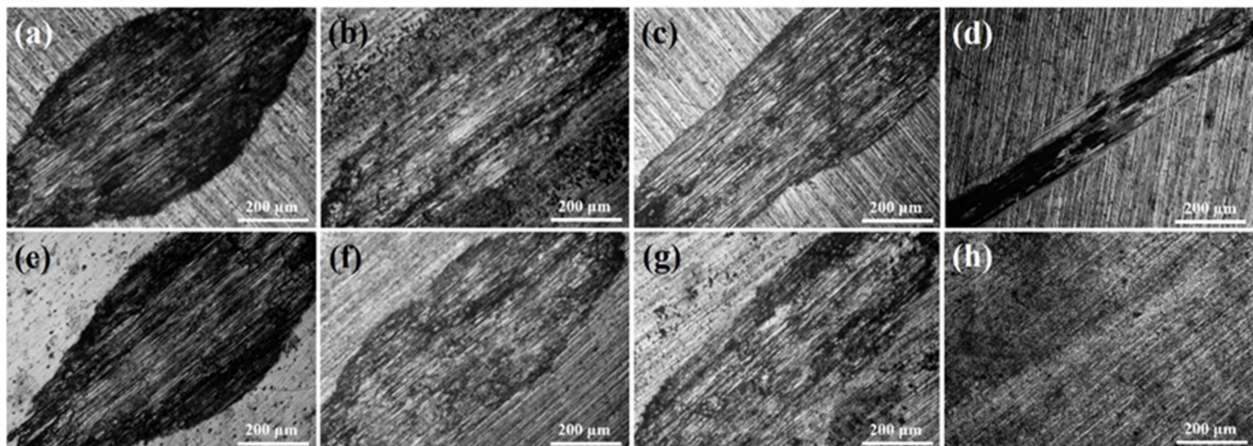


Figure 10. Worn surface morphologies of coatings observed by optical microscope: (a) as-deposited, (b) 200 °C annealed, (c) 400 °C annealed and (d) 600 °C annealed Ni-Mo coatings; and (e) as-deposited, (f) 200 °C annealed, (g) 400 °C annealed and (h) 600 °C annealed Ni-Mo coatings.

The further analysis of worn surface for representative as-deposited and 600 °C annealed Ni-Mo-W coatings is illustrated in Figure 11, respectively, which exhibits obvious grooves and debris within the morphologies at high magnification. For as-deposited, part of debris adheres to the worn surface under the action of compressive stress. EDS analysis results of debris (1 & 2 select locations) as listed in Table 3 display the existence of considerable content of Fe element, suggesting the transferring of adhesive debris between worn surfaces and corresponding counterparts. This indicates that the severe wear is subjected to as-deposited Ni-Mo-W coating and the subsistence of both adhesive and abrasive wear. As shown in Figure 11b, worn surface morphology of 600 °C annealed Ni-Mo-W coating demonstrates typical abrasion wear due to observation of plough grooves and abrasive particles. The micro-cracks are also observed with absorbing lubricants applied for improving the wear resistance [46]. It can be referred that the formation of a mixture of oxides such as NiO, Ni₄MoO₂ [47], MoO₃, and WO₃ [8] through the result of chemical composition (EDS) at select positions (3 & 4) on the worn surface, providing lubrication during abrasive worn process with lower friction coefficient and wear rate of 600 °C annealed Ni-Mo-W coating. This may be attributed that the localized friction heat at the asperity contact leads to oxidize the Ni(Mo,W) solution, even Ni₃Mo and Ni₄W intermetallic compounds with formation of oxide particles and cracks distributed in whole worn surface as evident from Figure 11b. Therefore, the wear resistance of coatings is improved eventually by formation of a mixture of lubricated oxides upon-annealing at 600 °C and the enhancement of H/E ratio for ≤ 400 °C annealed Ni-Mo-W coatings, respectively.

Table 3. The chemical composition acquired corresponding results of EDS spectra for the select locations in Figure 11.

Selected Locations	O (at.%)	Ni (at.%)	Mo (at.%)	W (at.%)	Fe (at.%)	Cr (at.%)
1	17.1	39.8	7.2	4.6	30.9	0.4
2	21.5	42.4	7.7	3.8	24.3	0.3
3	55.2	22.7	8.7	7.0	6.3	0.1
4	70.2	16.5	9.4	2.1	1.8	–

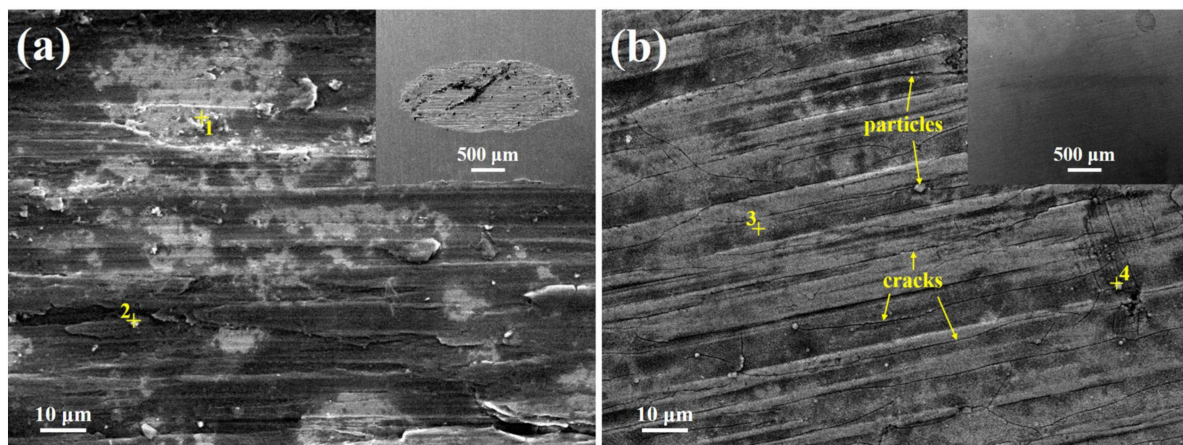


Figure 11. SEM micrographs of worn tracks and the select locations of corresponding EDS spectra for (a) as-deposited and (b) 600 °C annealed Ni-Mo-W coatings, and the corresponding morphologies at low magnification are shown in insets of (a,b), respectively.

4. Conclusions

In this study, an investigation on the influence of annealing at temperatures from 200 to 600 °C on microstructure and mechanical properties of Ni-Mo and Ni-Mo-W alloy coatings electrodeposited on stainless steel substrate was undertaken. It is found that, up to 400 °C, the Ni-Mo-W coatings mainly consist of nano-crystalline Ni-based solid solution with the average crystallite size lower than 30 nm. Compared with corresponding Ni-Mo coatings in same condition, the grains of coatings are refined with the coexistence of Mo-W elements and annealing heat treatment causes the slight grain growth. In addition, phase separation occurs with formation of Ni₄W and Ni₃Mo-Ni₄W intermetallic precipitates in the 400 °C annealed and 600 °C annealed Ni-Mo-W coatings, respectively. The Mo-W additions in coating and annealing heat treatment result in enhancement of the hardness of coatings significantly. The highest values of hardness and elastic module reach about 10.8 ± 0.6 GPa and 222 ± 7 GPa, respectively, due to strengthening effect of precipitated Ni₃Mo and Ni₄W particles corresponding to 600 °C annealed Ni-Mo-W coating. The wear resistance increases with the annealing temperature for both Ni-Mo and Ni-Mo-W coatings, which can be mainly attribute to the improvement of H/E ratio for ≤ 400 °C annealed Ni-Mo-W coatings and formation of a mixture of lubricated oxides upon-annealing at 600 °C, respectively. The combination of adhesive wear and abrasive wear are presented as the wear mechanism of Ni-Mo-W coatings, which are dominated by abrasive wear for 600 °C annealed coating. In conclusion, Ni-Mo-W coatings show excellent hardness and wear resistance upon post-annealing at elevated temperature.

Author Contributions: C.Z.: Project administration, Methodology, Investigation, Data analysis, Funding acquisition, Writing; W.S.: Data analysis; Y.W.: Writing—review & editing; S.D.: Literature search; D.S.: Supervision. All authors have read and agreed to the published version of the manuscript.

Funding: This work was financially supported by the Natural Science Foundation of Jiangsu Province (Grant No. BK20181027), the Innovative and Entrepreneurial Doctor Project of Jiangsu Province, and the Scientific Research Foundation of Nanjing Institute of Technology (Grant No. YKJ201709).

Institutional Review Board Statement: Not applicable.

Informed Consent Statement: Not applicable.

Data Availability Statement: The data that support the findings of this study are available within this article.

Acknowledgments: The authors would like to thank Shiyanjia Lab (www.shiyanjia.com) for the XRD analysis.

Conflicts of Interest: The authors declare no conflict of interest.

References

1. Cui, W.; Wang, K.; Wang, K.; Wang, P. Effects of jet rate on microstructure, microhardness, and wear behavior of jet electrodeposited Ni-SiC composites. *Ceram. Int.* **2018**, *44*, 7214–7220. [[CrossRef](#)]
2. Lelevic, A.; Walsh, F.C. Electrodeposition of NiP alloy coatings: A review. *Surf. Coat. Technol.* **2019**, *369*, 198–220. [[CrossRef](#)]
3. Shahzad, K.; Radwan, A.B.; Fayyaz, O.; Shakoob, R.A.; Uzma, M.; Umer, M.A.; Baig, M.N.; Raza, A. Effect of concentration of TiC on the properties of pulse electrodeposited Ni-P-TiC nanocomposite coatings. *Ceram. Int.* **2021**, *47*, 19123–19133. [[CrossRef](#)]
4. Torabinejad, V.; Aliofkhaezrai, M.; Rouhaghdam, A.S.; Allahyarzadeh, M.H. Tribological properties of Ni-Fe-Co multilayer coatings fabricated by pulse electrodeposition. *Tribol. Int.* **2017**, *106*, 34–40. [[CrossRef](#)]
5. Torabinejad, V.; Aliofkhaezrai, M.; Rouhaghdam, A.S.; Allahyarzadeh, M.H.; Kasama, T.; Alimadadi, H. Mechanical properties multilayer Ni-Fe and Ni-Fe-Al₂O₃ nanocomposite coating. *Mater. Sci. Eng. A-Struct.* **2017**, *700*, 448–456. [[CrossRef](#)]
6. Allahyarzadeh, M.H.; Aliofkhaezrai, M.; Rouhaghdam, A.S.; Alimadadi, H.; Torabinejad, V. Mechanical properties and load bearing capability of nanocrystalline nickel-tungsten multilayered coatings. *Surf. Coat. Technol.* **2020**, *386*, 125472. [[CrossRef](#)]
7. Dilek, S.; Algül, H.; Akyol, A.; Alp, A.; Akbulut, H.; Uysal, M. Pulse electro co-deposition of submicron-sized TiC reinforced Ni-W coatings: Tribological and corrosion properties. *J. Asian Ceram. Soc.* **2021**, *9*, 673–685. [[CrossRef](#)]
8. Wasekar, N.P.; Verulkar, S.; Vamsi, M.V.N.; Sundararajan, G. Influence of molybdenum on the mechanical properties, electrochemical corrosion and wear behavior of electrodeposited Ni-Mo alloy. *Surf. Coat. Technol.* **2019**, *370*, 298–310. [[CrossRef](#)]
9. Mousavi, R.; Bahrololoom, M.E.; Deflorian, F. Preparation, corrosion, and wear resistance of Ni-Mo/Al composite coating reinforced with Al particles. *Mat. Des.* **2016**, *110*, 456–465. [[CrossRef](#)]
10. Wasekar, N.P.; Sundararajan, G. Sliding wear behavior of electrodeposited Ni-W alloy and hard chrome coatings. *Wear* **2015**, *342*, 340–348. [[CrossRef](#)]
11. Lv, J.; Wang, Z.; Liang, T.; Ken, S.; Miura, H. Effect of tungsten on microstructures of annealed electrodeposited Ni-W alloy and its corrosion resistance. *Surf. Coat. Technol.* **2018**, *337*, 516–524.
12. Wang, H.; Liu, R.; Cheng, F.J.; Cao, Y.; Ding, G.F.; Zhao, X.L. Electrodepositing amorphous Ni-W alloys for MEMS. *Microelectron. Eng.* **2010**, *87*, 1901–1906. [[CrossRef](#)]
13. Yin, D.; Marvel, C.J.; Cui, F.Y.; Vinci, R.P.; Harmer, M.P. Microstructure and fracture toughness of electrodeposited Ni-21 at.% W alloy thick films. *Acta Mater.* **2018**, *143*, 272–280. [[CrossRef](#)]
14. Suresha, S.J.; Haj-Taieb, M.; Bade, K.; Aktaa, J.; Hemker, K.J. The influence of tungsten on the thermal stability and mechanical behavior of electrodeposited nickel MEMS structures. *Scr. Mater.* **2010**, *63*, 1141–1144. [[CrossRef](#)]
15. Allahyarzadeh, M.H.; Aliofkhaezrai, M.; Rezvanian, A.R.; Torabinejad, V.; Rouhaghdam, A.R.S. Ni-W electrodeposited coatings: Characterization, properties and applications. *Surf. Coat. Technol.* **2016**, *307*, 978–1010. [[CrossRef](#)]
16. Sim, G.D.; Krogstad, J.A.; Reddy, K.M.; Xie, K.Y.; Valentino, G.M.; Weihs, T.P.; Hemker, K.J. Nanotwinned metal MEMS films with unprecedented strength and stability. *Sci. Adv.* **2017**, *3*, e1700685. [[CrossRef](#)]
17. Valentino, G.M.; Krogstad, J.A.; Weihs, T.P.; Hemker, K.J. Tailoring the coefficient of thermal expansion of ternary nickel alloys through compositional control and non-contact measurements. *J. Alloys Compd.* **2020**, *833*, 155024. [[CrossRef](#)]
18. Mosayebi, S.; Rezaei, M.; Mahidashti, Z. Comparing corrosion behavior of Ni and Ni-Mo electroplated coatings in chloride mediums. *Colloids Surf. A* **2020**, *594*, 124654. [[CrossRef](#)]
19. Allahyarzadeh, M.H.; Roozbehani, B.; Ashrafi, A.; Shadizadeh, S.R. Electrodeposition of high Mo content amorphous/nanocrystalline Ni-Mo alloys using 1-methyl-imidazolium chloride ionic liquid as an additive. *Surf. Coat. Technol.* **2011**, *206*, 137–142. [[CrossRef](#)]
20. Liu, J.H.; Yan, J.X.; Pei, Z.L.; Gong, J.; Sun, C. Effects of Mo content on the grain size, hardness and anti-wear performance of electrodeposited nanocrystalline and amorphous Ni-Mo alloys. *Surf. Coat. Technol.* **2020**, *404*, 126476. [[CrossRef](#)]
21. Laszczyńska, A.; Winiarski, J.; Szczygiel, B.; Szczygiel, I. Electrodeposition and characterization of Ni-Mo-ZrO₂ composite coatings. *Appl. Surf. Sci.* **2016**, *369*, 224–231. [[CrossRef](#)]
22. Xu, Y.; Ma, S.; Fan, M.; Chen, Y.; Song, X.; Hao, J. Design and properties investigation of NiMo composite coating reinforced with duplex nanoparticles. *Surf. Coat. Technol.* **2019**, *363*, 51–60. [[CrossRef](#)]
23. Alizadeh, M.; Cheshmpish, A. Electrodeposition of Ni-Mo/Al₂O₃ nano-composite coatings at various deposition current densities. *Appl. Surf. Sci.* **2019**, *466*, 433–440. [[CrossRef](#)]
24. Liu, J.H.; Pei, Z.L.; Shi, W.B.; Liu, Y.D.; Gong, J.; Sun, C. Studies on preparation, microstructure, mechanical properties and corrosion resistance of Ni-Mo/micron-sized diamond composite coatings. *Surf. Coat. Technol.* **2020**, *385*, 125451. [[CrossRef](#)]
25. Fan, J.; Cui, S.; Chen, J.; Liu, K.; Han, Q. Electrochemical properties of pulse plating amorphous Ni-Mo-W alloy coating in alkaline medium. *Rare Metal Mat. Eng.* **2015**, *44*, 538–543.
26. Allam, M.; Benaicha, M.; Dakhouche, A. Electrodeposition and characterization of NiMoW alloy as electrode material for hydrogen evolution in alkaline water electrolysis. *Int. J. Hydrog. Energ.* **2018**, *43*, 3394–3405. [[CrossRef](#)]
27. Liu, J.H.; Li, W.H.; Pei, Z.L.; Gong, J.; Sun, C. Investigations on the structure and properties of nanocrystalline Ni-Mo alloy coatings. *Mater. Charact.* **2020**, *167*, 110532. [[CrossRef](#)]
28. Wang, J.; Han, L.; Li, X.; Huang, Y.; Liu, Y.; Wang, Z. Temperature-dependent evolution of strength of nanocrystalline Ni(Mo) alloys at the Mo solubility limit. *Mat. Sci. Eng. A-Struct.* **2020**, *786*, 139326. [[CrossRef](#)]

29. Kapoor, G.; Péter, L.; Fekete, É.; Lábár, J.L.; Gubicza, J. The influence of Mo addition on the microstructure and its thermal stability for electrodeposited Ni films. *Mater. Charact.* **2018**, *145*, 563–572. [[CrossRef](#)]
30. Bigos, A.; Janusz-Skuza, M.; Szczerba, M.J.; Kot, M.; Zimowski, S.; Dębski, A.; Beltowska-Lehman, E. The effect of heat treatment on the microstructural changes in electrodeposited Ni-Mo coatings. *J. Mater. Process. Technol.* **2020**, *276*, 116397. [[CrossRef](#)]
31. Liu, J.H.; Yan, J.X.; Liu, Y.D.; Li, W.H.; Gu, W.S.; Pei, Z.L.; Gong, J.; Sun, C. Impact of annealing temperature on the microstructure, microhardness, tribological properties and corrosion resistance of Ni-Mo/diamond composites. *Appl. Surf. Sci.* **2021**, *541*, 148367. [[CrossRef](#)]
32. Vamsi, M.V.N.; Wasekar, N.P.; Sundararajan, G. Influence of heat treatment on microstructure and mechanical properties of pulse electrodeposited Ni-W alloy coatings. *Surf. Coat. Technol.* **2017**, *319*, 403–414. [[CrossRef](#)]
33. Holzwarth, U.; Gibson, N. The Scherrer equation versus the ‘Debye-Scherrer equation’. *Nat. Nanotechnol.* **2011**, *6*, 534. [[CrossRef](#)] [[PubMed](#)]
34. Oliver, W.C.; Pharr, G.M. An improved technique for determining hardness and elastic modulus using load and displacement sensing indentation experiments. *J. Mater. Res.* **1992**, *7*, 1564–1583. [[CrossRef](#)]
35. Zmitrowicz, A. Wear patterns and laws of wear—a review. *Theor. Appl. Mech.* **2006**, *44*, 219–253.
36. Sun, S.; Bairachna, T.; Podlaha, E.J. Induced codeposition behavior of electrodeposited NiMoW alloys. *J. Electrochem. Soc.* **2013**, *160*, D434–D440. [[CrossRef](#)]
37. Rupert, T.J.; Trelewicz, J.R.; Schuh, C.A. Grain boundary relaxation strengthening of nanocrystalline Ni-W alloys. *J. Mater. Res.* **2012**, *27*, 1285–1294. [[CrossRef](#)]
38. Detor, A.J.; Schuh, C.A. Tailoring and patterning the grain size of nanocrystalline alloys. *Acta Mater.* **2007**, *55*, 371–379. [[CrossRef](#)]
39. Schuh, C.A.; Nieh, T.G.; Iwasaki, H. The effect of solid solution W additions on the mechanical properties of nanocrystalline Ni. *Acta Mater.* **2003**, *51*, 431–443. [[CrossRef](#)]
40. Yamasaki, T.; Schloßmacher, P.; Ehrlich, K.; Ogino, Y. Formation of amorphous electrodeposited Ni-W alloys and their nanocrystallization. *Nanostruct. Mater.* **1998**, *10*, 375–388. [[CrossRef](#)]
41. Szajewski, B.A.; Crone, J.C.; Knap, J. Analytic model for the Orowan dislocation-precipitate bypass mechanism. *Materialia* **2020**, *11*, 100671. [[CrossRef](#)]
42. De Jong, M.; Chen, W.; Angsten, T.; Jain, A.; Notestine, R.; Gamst, A.; Sluiter, M.; Ande, C.K.; van der Zwaag, S.; Plata, J.J.; et al. Charting the complete elastic properties of inorganic crystalline compounds. *Sci. Data* **2015**, *2*, 150009. [[CrossRef](#)]
43. Leyland, A.; Matthews, A. On the significance of the H/E ratio in wear control: A nanocomposite coating approach to optimised tribological behavior. *Wear* **2000**, *246*, 1–11. [[CrossRef](#)]
44. Zhai, W.; Bai, L.; Zhou, R.; Fan, X.; Kang, G.; Liu, Y.; Zhou, K. Recent progress on wear-resistant materials: Designs, properties, and applications. *Adv. Sci.* **2021**, *8*, 2003739. [[CrossRef](#)]
45. Vamsi, M.V.N.; Wasekar, N.P.; Sundararajan, G. Sliding wear of as-deposited and heat-treated nanocrystalline nickel-tungsten alloy coatings. *Wear* **2018**, *412*, 136–143. [[CrossRef](#)]
46. Aliofkhaezai, M.; Walsh, F.C.; Zangari, G.; Köçkar, H.; Alper, M.; Rizal, C.; Magagnin, L.; Protsenko, V.; Arunachalam, R.; Rezvanian, A.; et al. Development of electrodeposited multilayer coatings: A review of fabrication, microstructure, properties and applications. *Appl. Surf. Sci. Adv.* **2021**, *6*, 100141. [[CrossRef](#)]
47. Woydt, M.; Skopp, A.; Dorfel, I.; Witke, K. Wear engineering oxides/antiwear oxides. *Tribol. Trans.* **1999**, *42*, 21–31. [[CrossRef](#)]